# A Tuned Whitening-based Taylor-Kalman Filter for P Class Phasor Measurement Units

Amir Bashian, David Macii, *Senior Member*, *IEEE*, Daniele Fontanelli, *Senior Member*, *IEEE*, Dario Petri, *IEEE Fellow, IEEE*

***Abstract* — Protection-oriented (P Class) Phasor Measurement Units (PMUs) are required to reconcile high measurement accuracy and low latency in order to promptly detect possible anomalous operating conditions in power systems. Most of the existing estimators of synchrophasor magnitude, phase, frequency and Rate of Change of Frequency (ROCOF) of voltage or current AC waveforms need to acquire the samples of at least two power line cycles to meet the P Class requirements specified in the IEEE/IEC Standard 60255-118-1:2018. In this paper instead, a multistep technique based on the combination of Multiple Signal Classification (MUSIC), narrowband disturbance whitening and Taylor-Kalman Filtering (TKF) is proposed to maximize accuracy even over one-cycle-long observation intervals. Both MUSIC and disturbance whitening rely on a common theoretical framework (i.e., signal and noise vector subspace decomposition) and they are applied to compensate for the detrimental effect of off-nominal frequency deviations and harmonic distortion, respectively. The use of a cascaded dynamic estimators such as the TKF is motivated by the need to track possible in-band amplitude and phase oscillations or step-like changes with low latency. While the basic TKF is very sensitive to possible narrowband disturbances, the Tuned Whitening-based Taylor-Kalman filter (TW-TKF) described in this paper ensures superior accuracy under the influence of harmonics and amplitude or phase step changes, with just a minor performance degradation in the other P Class testing conditions reported in the IEEE/IEC Standard 60255-118-1:2018.**

***Keywords* — phasor measurement units (PMUs), power system monitoring, Signal processing, Kalman filtering. smart grid measurements.**

## I. Introduction

The growing penetration of distributed generators and dynamic loads poses new challenges for low-voltage (LV) and medium-voltage (MV) network operation [1]. To handle possible critical time-varying operating conditions such as, for instance, supply-demand fluctuations, supply volatility or topology changes, the state of the grid should be estimated in real-time [2]. To this end, the so-called Wide Area Monitoring Systems (WAMS) are equipped with an adequate number of properly placed Phasor Measurement Units (PMUs) [3]–[5]. PMUs are particularly useful to support system state estimation as well as to detect possible impending faults, since they are able to estimate the phasors of voltage and current AC signals at a high rate and over a time scale synchronized with the Coordinated Universal Time (UTC). Unfortunately, the measurement of magnitude, phase, frequency, and the Rate of Change of Frequency (ROCOF) of AC waveforms is affected by a variety of uncertainty contributions, especially when short observation intervals are considered. For this reason, several estimation algorithms for PMUs have been recently proposed in the scientific literature [6]-[7].

The IEEE/IEC Standard 60255-118-1:2018 (briefly referred to as "the IEEE/IEC Standard" in the rest of this paper) specifies two classes of PMUs depending on the purpose for which they are used [8]. For applications requiring superior accuracy, the so-called Measurement-class (or *M Class*) PMUs are needed. However, for protection purposes a lower accuracy is acceptable provided that the estimation latencies are as short as possible. For this kind of applications, the so-called *P Class* requirements are specified in the IEEE/IEC Standard. Either PMU class must comply with its own set of performance limits expressed in terms of *Total Vector Errors* (TVE), *Frequency Errors* (FE), *Rate of change of Frequency Errors* (RFE). Moreover, in the case of amplitude or phase abrupt changes, also response and delay times have to be evaluated. Even though the limits reported in the IEEE/IEC Standard were established mainly for transmission systems monitoring, at the moment they are usually a reference also for distribution-level PMUs. However, the inherent characteristics of distribution systems (e.g., the use of shorter lines with a lower *X/R* ratio than in transmission systems [9]) as well the presence of stronger harmonic and inter-harmonic interferers caused by a variety of sources pose two further crucial and contrasting problems [10]. On one hand, the phase angle differences between bus voltage phasors are very small (in the order of a few mrad) [11], which requires higher accuracy than traditional PMUs. On the other hand, the presence of larger disturbances makes this task extremely challenging especially when short data records are considered.

This paper provides a partial response to the problems above by proposing a multistep estimator, called *Tuned Whitening-based Taylor-Kalman Filter* (TW-TKF), that is able to greatly mitigate the uncertainty contributions due to both off-nominal system frequency deviations and large harmonic distortion even over one-cycle-long observation intervals. The TW-TKF results from an extension of the *Whitening-based Taylor-Kalman Filter* (W-TKF) presented in [12], and it outperforms both the W-TKF and the basic TKF in the most critical testing conditions reported in the IEEE/IEC Standard. Since the whitening technique used to decorrelate possible narrowband interferers tends to desensitize the TKF ability to track dynamic magnitude and/or angle phasor oscillations as the observation intervals length grows, the proposed technique is particularly effective over short intervals and, consequently, for *P Class* PMUs.

The rest of the paper is structured as follows. In Section II, a presentation of the related work is reported to highlight the key advantages and the differences of the proposed algorithm compared with other techniques. In Section III, the steps of the TW-TKF method are described in detail. In Section IV the results of multiple simulations in a variety of testing conditions

(most of which are reported in the IEEE/IEC Standard) are reported and compared with those obtained with both the basic TKF and the W-TKF presented in [12]. In Section V some experimental results in different steady-state and transient conditions are shown. Finally, in Section VI the main conclusions are summarized.

## II. Related Work and Motivations

The tight accuracy requirements of next–generation PMUs are not the only reason why the related measurement problem is so challenging. A further, subtler reason is that two contrasting goals have to be pursued at the same time. On one hand, the impact of off-nominal frequency deviations and steady-state harmonic and inter-harmonic disturbances on the estimation of the parameter of the fundamental component has to be made negligible. On the other hand, possible time-varying changes of these parameters should be tracked quickly and accurately. In addition, the wideband noise (which, although always present, is basically disregarded in the IEEE/IEC Standard) may have unpleasant consequences on performances, especially on ROCOF estimation accuracy [13].

The steady-state uncertainty contributions can be effectively mitigated with a low computational burden by using the signal quadrature demodulation approach followed by low-pass filtering suggested in the Annex D of the IEEE/IEC Standard [8]. This technique was implemented by using a variety of filters [14]–[16]. Alternatively, several frequency-domain estimators based on the Discrete Fourier Transform (DFT) can be used [17]–[19]. In order to provide adequate accuracy, both kinds of estimators require to sample and to process the input AC waveform over multiple power line cycles. In the former case, linear-phase digital filters with a finite impulse response in the order of a few cycles are needed to ensure a narrow transition bandwidth and a high out-of-band attenuation. In the latter case, a quite broad variety of DFT-based algorithms designed to counteract the detrimental impact of different disturbances is reported in the scientific literature. For instance, in [18], [20] auxiliary down-sampling or filtering techniques are used to mitigate the influence of possible DC decaying offsets. The interpolated DFT (IpDFT) is very accurate in estimating static off-nominal frequency deviations and to correct synchrophasor magnitude and phase accordingly [21]. Similar results can be obtained if the fundamental frequency is estimated with an ad-hoc transducer prior to computing the discrete-time Fourier transform of the acquired signal [22]. Enhanced two-step versions of the basic IpDFT can be used to correct the estimation errors caused by the spectral infiltration of the fundamental image component and/or the second-order harmonic [17], [19]. A similar idea can be extended to remove iteratively all harmful narrowband components (including the inter-harmonic tones) from the signal spectrum [23]. However, all the aforementioned techniques suffer from common problems. In particular, they return accurate results only when steady-state disturbances affect the fundamental tone and multiple power line cycles are acquired. In fact, their accuracy and responsiveness tend to degrade when dynamic disturbances (e.g., amplitude and/or phase oscillations or steps) occur. On the contrary, under time-varying operating conditions, measurements over short observation intervals are preferable to better track AC voltage or current parameters variations. Unfortunately, when data records no longer than two power line cycles are processed, the performance of DFT-based techniques in some testing conditions may become unacceptable. To address this problem, several algorithms based on the Taylor's series expansion of the function describing the synchrophasor time evolution exist [24]. One of the most effective solutions is the so-called Taylor's series-based Weighted Least Squares (TWLS) estimator, also known as Taylor-Fourier Filter [25]. However, it is sensitive to possible off-nominal static frequency deviations unless their value is first estimated (e.g., through a preliminary IpDFT) and then used to correct the coefficients of the system of equations returning the WLS estimate of Taylor's series coefficients [26], [27]. In addition, when low-order harmonics or inter-harmonics affect the signal, the TWLS estimation accuracy can decrease considerably. Relevant improvements can be obtained, although at the expense of a higher computational burden, if the parameters of the narrowband disturbances are included in the set of variables to be estimated. This approach is adopted for instance in the so-called Taylor-Fourier Transform (which includes the harmonics phasors) [28], or in the algorithms based on the compressed sensing Taylor-Fourier multifrequency model [29]. However, also in this case achieving high accuracy requires the acquisition of signal samples over multiple cycles.

In such conditions, the techniques based on signal and noise subspace decomposition, particularly the Multiple Signal Classification (MUSIC) or the Estimation of Signal Parameters via Rotational Invariant Techniques (ESPRIT) are particularly effective for frequency estimation even in the presence of multi-tone disturbances [30]-[31]. For this reason, various subspace-based techniques were also developed for PMU applications [32]-[33]. The main drawback of such solutions is that if the number of sinusoidal components is unknown a priori, it must be estimated heuristically from the available data. However, most of the criteria proposed in the literature to distinguish the eigenvalues associated with the sinusoidal components from those of the noise subspace are affected by severe robustness problems, especially in time-varying operating conditions.

The technique proposed in this paper also relies on the idea of estimating the signal fundamental frequency through a subspace-based approach (i.e., a lightweight MUSIC version) prior to performing synchrophasor estimation. However, the proposed method reverses the perspective of other research works because, instead of using the signal subspace decomposition to estimate the narrowband disturbances, it makes use of the same theoretical background to transform them into wideband noise. In this way, the delicate problem of estimating the number of sinusoidal components of the signal disappears. The idea of harmonics whitening through a subspace-based decorrelation is not totally new, as it was for the first time introduced in [34]. However, that paper presents just a preliminary study on the feasibility of disturbance whitening using the classic TWLS estimator as a benchmark.

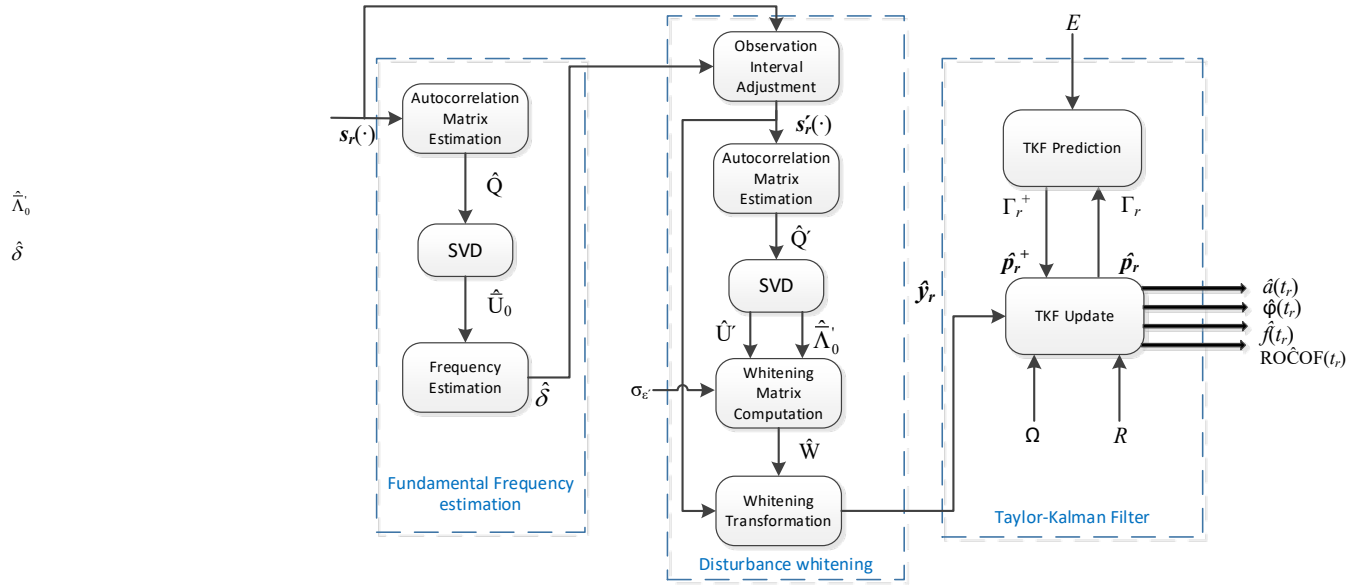


Fig. 1. Block diagram of the proposed TW-TKF algorithm.

In this paper instead the whitening performances are improved in two ways, i.e. i) by adjusting the observation interval length in order to use only the samples that belong to one or two full power line cycles, regardless of possible off-nominal frequency deviations and ii) by replacing the noise subspace eigenvalues with much lower values to improve signal spectral purity. Both such solutions improve the accuracy of the original W-TKF algorithm [12].

Once the input signal is cleaned up from steady-state disturbances, synchrophasor magnitude, phase, frequency and ROCOF are estimated through a TKF, namely a Kalman a filter in which the vector of state variables includes the Taylor's series coefficients of the fundamental synchrophasor. The rationale for this choice is that Kalman filters are natively conceived to track possible time-varying changes of the state variables. Indeed, various single-phase or three-phase Kalman filters or extended Kalman filters for PMUs have been proposed over the last few years [35]–[39]. Unfortunately, the estimates returned by Kalman filters can be strongly sensitive to harmonics if they are not included in the signal model [35]. Since in the proposed approach all sinusoidal disturbances are strongly mitigated by the preliminary whitening step, and recalling that Kalman filters are formally optimal in rejecting the input white noise, the use of a TKF after whitening looks a promising approach to achieve an excellent trade-off between estimation accuracy and responsiveness for *P Class* PMUs.

## III. Signal Model and TW-TKF Algorithm Description

A generic AC voltage or current waveform can be modelled as follows, i.e.

$$s(t) = x(t) + d(t) + \varepsilon(t) = a(t)\cos\left[2\pi f_0 t + \varphi(t)\right] + d(t) + \varepsilon(t) \quad (1)$$

where:

- $a(t)$ and $\varphi(t)$ are the time-varying amplitude and phase, respectively, of the ideal fundamental sinewave $x(t)$;
- $f_0 = f_{\text{nom}} \cdot (1 + \delta)$ is the fundamental power system frequency, which may deviate from the nominal value $f_{\text{nom}}$ (i.e., 50 Hz or 60 Hz) by a relative offset $\delta$, e.g., due to a mismatch between power demand and supply;
- $d(t)$ includes the sum of all sinusoidal disturbances;
- $\varepsilon(t)$ is a white and normally distributed noise floor with zero-mean and variance $\sigma_\varepsilon^2$.

The synchrophasor $p(t_r) = \frac{a(t_r)}{\sqrt{2}} e^{j\varphi(t_r)}$, the instantaneous frequency $f(t_r) = f + \frac{1}{2\pi}\frac{d\varphi(t)}{dt}\Big|_{t_r}$ and the ROCOF $\frac{df}{dt}\Big|_{t_r} = \frac{1}{2\pi}\frac{d^2\varphi(t)}{dt^2}\Big|_{t_r}$ values of $x(t)$ have to be estimated at the UTC reference time $t_r$. Assuming that:

- $M = [f_s/f_{\text{nom}}]$ represents the integer number of samples per nominal power line cycle, where $f_s$ is the PMU sampling rate and $[\cdot]$ the "rounding to the nearest integer" operator;
- $C$ is the integer number of nominal cycles that are acquired in each observation interval;

then the size of the data record used to estimate the synchrophasor magnitude, phase, frequency and ROCOF is $N = M \cdot C$ or $N = M \cdot C + 1$ depending on whether $M \cdot C$ is odd or even, respectively. In this way, if $t_r$ lies in the center of each observation interval, the reference time coincides with the time of the central sample and the sequence of acquired samples can be simply expressed as

$$s(n_r) = a(n_r)\cos\left[\omega_0 n_r + \varphi(n_r)\right] + d(n_r) + \varepsilon(n_r) \quad (2)$$

where $\omega_{\text{nom}} = 2\pi\frac{f_{\text{nom}}}{f_s} \approx \frac{2\pi}{M}$, $r - \frac{N-1}{2} \le n_r \le r + \frac{N-1}{2}$ and $r = t_r \cdot f_s$. The block diagram of the TW-TKF algorithm processing the samples of data record (2) is shown in Fig. 1. In the following subsections, the steps of the algorithm are described in detail.

### A. Fundamental frequency estimation real-valued MUSIC

Let us assume that $d(t)$ in (1) and (2) consists of $D$ significant sinusoidal disturbances emerging from the noise floor with

$N > 2D+2$ (which is a condition easily met in the application considered) [40]. If $\boldsymbol{s}_r(m)$ is the column vector consisting of the values of (2) included within the interval $\left[m+r-\frac{N-1}{2}, m+r+\frac{N-1}{2}\right]$ for $m=-N+1,...,0$, the columns of the matrix $S_r=\left[\boldsymbol{s}_r(-N+1) \quad \boldsymbol{s}_r(-N+2) \quad \dots \quad \boldsymbol{s}_r(0)\right]$ consist of $N$ data each and they are shifted by one sample at a time till covering two subsequent observation intervals of size $N$. If $Q=E\left\{\boldsymbol{s}_r(\cdot)\boldsymbol{s}_r^T(\cdot)\right\}$ is the autocorrelation matrix of $\boldsymbol{s}_r(\cdot)$, in stationary conditions $Q$ is independent of $m$. Moreover, if the eigenvalues resulting from the Singular Value Decomposition (SVD) of $Q$ are arranged in a descending order and the corresponding eigenvectors are reordered accordingly, then $Q$ can be expressed as [31]

$$Q=U\Lambda U^{\mathrm{T}}=\begin{bmatrix}U_0 & \bar{U}_0\end{bmatrix}\begin{bmatrix}\Lambda_0 & 0\\ 0 & \bar{\Lambda}_0\end{bmatrix}\begin{bmatrix}U_0^{\mathrm{T}}\\ \bar{U}_0^{\mathrm{T}}\end{bmatrix}= \\ =\sum_{d=0}^{D}F(\omega_d)\left[\Lambda_d-\sigma_\varepsilon^2 I_N\right]F^{\mathrm{T}}(\omega_d)+\sigma_\varepsilon^2 I_N \tag{3}$$

where:

- $^{\mathrm{T}}$ is the transpose operator;
- $U$ is an $N \times N$ orthogonal matrix whose columns are the eigenvectors of $Q$ (hence $U^{-1}=U^{\mathrm{T}}$);
- $\Lambda$ is the diagonal matrix of the eigenvalues of $Q$;
- $\Lambda_0$ is $2 \times 2$ diagonal submatrix including the eigenvalues related to the fundamental tone, which are proportional to its power [30]-[31], and $U_0$ is the $N \times 2$ submatrix of the corresponding eigenvectors;
- $\bar{\Lambda}_0$ and $\bar{U}_0$ are the submatrices including the eigenvalues and eigenvectors, respectively, associated with all the other components of signal (2). In particular, recalling that $D$ sinusoidal disturbances affect (2), the $(N\text{-}2) \times (N\text{-}2)$ diagonal matrix $\bar{\Lambda}_0$ can be rewritten as [31],

$$\bar{\Lambda}_0=\begin{bmatrix}\Lambda_s & 0\\ 0 & \sigma_\varepsilon^2 I_{N-2D-2}\end{bmatrix} \tag{4}$$

  where $\Lambda_s=\mathrm{diag}(\Lambda_1,\dots,\Lambda_D)$ is a block diagonal matrix consisting of $2 \times 2$ diagonal submatrices whose elements are the eigenvalues proportional to the power of the related sinusoidal disturbance, and $I$ is the identity matrix of size $N$-2$D$-2, as specified in the subscript.
- Finally,

$$F(\omega_d)=\sqrt{\frac{2}{N}}\begin{bmatrix}\cos\left(-\omega_d(N-1)\right) & -\sin\left(-\omega_d(N-1)\right)\\ \cos\left(-\omega_d(N-2)\right) & -\sin\left(-\omega_d(N-2)\right)\\ \vdots & \vdots\\ 1 & 0\end{bmatrix}, \tag{5}$$

  and $\omega_d$ for $d$=0, …, $D$, is the (usually unknown) normalized frequency of the $d$-th sinusoidal component in (2), including the fundamental one (for $d$=0).

In practice $Q$ has to be estimated from the limited amount of data of two consecutive observation intervals, i.e.

$$\hat{Q}=\frac{1}{N}S_r\cdot S_r^{\mathrm{T}}=\hat{U}\hat{\Lambda}\hat{U}^{\mathrm{T}}=\begin{bmatrix}\hat{U}_0 & \hat{\bar{U}}_0\end{bmatrix}\begin{bmatrix}\hat{\Lambda}_0 & 0\\ 0 & \hat{\bar{\Lambda}}_0\end{bmatrix}\begin{bmatrix}\hat{U}_0^{\mathrm{T}}\\ \hat{\bar{U}}_0^{\mathrm{T}}\end{bmatrix} \tag{6}$$

where symbol "$\hat{\cdot}$" denotes an estimated quantity. Therefore, the estimation uncertainty associated with $\hat{Q}$ propagates to eigenvalues and eigenvectors returned by the SVD.

In general, the MUSIC algorithm for real-valued sinewaves was conceived to estimate the frequency of all sinusoidal components in (2) assuming that the value of $D$ is known a priori [31]. However, such a strong assumption is not needed in the specific case at hand because of two reasons. Firstly, we are interested in estimating just the frequency of the fundamental tone both for observation interval adjustment and to tune the elements of the TKF output matrix in the update step (see Sections III.B and III.C). Secondly, all the narrowband disturbances are supposed to be cancelled or at least strongly mitigated by the following whitening step.

To determine the unknown frequencies through MUSIC, just the noise eigenvectors must be known [31]. However, the whitening transformation (see Appendix A) is designed to change only the eigenvalues, while preserving the eigenvectors of the signal and noise subspaces. Therefore, the elements of the matrix $U$ in principle do not change after disturbance whitening. As a consequence, even if the value of $D$ is unknown and the actual size of the noise subspace before disturbance whitening is lower than $\bar{U}_0$, the real-valued matrix equation $F^T(\omega_0)\bar{U}_0\bar{U}_0^{\mathrm{T}}F(\omega_0)=0$ (that has to be solved to determine the spectral peak at frequency $\omega_0$) certainly converges to a solution. Unfortunately, considering that in practice matrix $\bar{U}_0$ is estimated through (6), a zero of the matrix function $F^T(\omega_0)\bar{U}_0\bar{U}_0^{\mathrm{T}}F(\omega_0)$ can be hardly found.

Therefore, the real-valued MUSIC estimator of the fundamental normalized frequency is [31]

$$\hat{\omega}_0=\arg\min_{\omega\in BW}\left\{\mathrm{tr}[F^T(\omega_0)\hat{\bar{U}}_0\hat{\bar{U}}_0^{\mathrm{T}}F(\omega_0)]\right\} \tag{7}$$

where the operator tr[·] returns the trace of the argument matrix, $BW=\left[\omega_{\mathrm{nom}}-\frac{\delta_{\max}}{M}, \omega_{\mathrm{nom}}+\frac{\delta_{\max}}{M}\right]$ is the interval where the normalized frequency is supposed to lie, and $\delta_{\max}$ is the maximum allowed off-nominal frequency deviation. It is important to emphasize that the computational burden of MUSIC is generally demanding (see Section III.D). Moreover, it depends on both the number of frequency components to be estimated and on the width of the frequency range to explore. However, in the case at hand the computation of (7) is lightweight because just the fundamental frequency has to be estimated and the interval $BW$ is very narrow. Therefore, any solver of (7) properly initialized to $\omega_{\mathrm{nom}}$ shall quickly converge to the desired solution. The corresponding estimated static off-nominal frequency deviation is then given by $\hat{\delta}=M\cdot(\hat{\omega}-\omega_0)$.

### *B. Observation interval adjustment and disturbance whitening*

The value of $\hat{\delta}$ can be used to adjust the length of the intervals over which both disturbance whitening and

synchrophasor estimation are performed. The purpose of this step is to select just the samples of an integer number of *actual* fundamental power line cycles, thus ensuring a quasi-coherent sampling of the input signal. In particular, the length of vectors $\boldsymbol{s}_r(\cdot)$ and the size of the matrix $S_r$ become equal to $\hat{N}=\left\lfloor \frac{N}{1+\hat{\delta}} \right\rfloor$ or $\hat{N}=\left\lfloor \frac{N}{1+\hat{\delta}} \right\rfloor+1$, depending on whether $\left\lfloor \frac{N}{1+\hat{\delta}} \right\rfloor$ is odd or even, respectively. If $\boldsymbol{s}'_r(\cdot)$ and $S'_r$ denote the array of data over the adjusted observation intervals, similarly to (3), the SVD of the autocorrelation matrix $Q' = E\left\{\boldsymbol{s}'_r(\cdot)\boldsymbol{s}'^T_r(\cdot)\right\}$ can be expressed as

$$Q' = U'\Lambda' U'^T = \begin{bmatrix} U'_0 & \bar{U}'_0 \end{bmatrix} \begin{bmatrix} \Lambda_0 & 0 \\ 0 & \bar{\Lambda}'_0 \end{bmatrix} \begin{bmatrix} U_0^{\mathrm{T}} \\ \bar{U}_0^{\mathrm{T}} \end{bmatrix} \tag{8}$$

where

$$\bar{\Lambda}'_0 = \begin{bmatrix} \Lambda_s & 0 \\ 0 & \sigma_\varepsilon^2 I_{\hat{N}-2D-2} \end{bmatrix}. \tag{9}$$

Observe that the elements of $U'_0$, $\bar{U}'_0$ and $\bar{\Lambda}'_0$ almost coincide with those of $U_0$, $\bar{U}_0$ and $\bar{\Lambda}_0$, respectively, the only difference being their size. However, submatrices $\Lambda_0$ and $\Lambda_s$ are exactly the same as those in (3) and (4). In particular, the two eigenvalues in $\Lambda_0$ can be easily identified since they are undoubtedly the greatest ones. The elements of $\Lambda_s$ can instead be replaced by those of an artificial noise subspace, while preserving the respective eigenvectors. In this way, all the sinusoidal components different from the fundamental one (regardless of their number) are transformed into white noise instead of being estimated, which is the opposite of the goal of most common subspace-based techniques.

As explained in details in [34] and recalled briefly in Appendix A, both disturbance whitening and wideband noise reduction can be achieved by applying the linear transformation

$$\hat{\boldsymbol{y}}_r = \hat{W}\,\boldsymbol{s}'_r \tag{10}$$

where $\boldsymbol{s}'_r$ represents, for the sake of brevity, the most recent vector of samples, i.e. $\boldsymbol{s}'_r(0)$, and

$$\hat{W} = \hat{U}' \begin{bmatrix} I_2 & 0 \\ 0 & \sigma'_\varepsilon \hat{\bar{\Lambda}}'^{-\frac{1}{2}}_0 \end{bmatrix} \hat{U}'^{\mathrm{T}} \tag{11}$$

is the estimated whitening matrix, in which $\sigma'_\varepsilon$ is the standard deviation of the zero-mean artificial wideband noise that is used to replace both the eigenvalues of the sinusoidal disturbances and those of the original noise subspace after the PMU acquisition stage and before synchrophasor estimation. Quite importantly, matrices $\hat{U}'$ and $\hat{\bar{\Lambda}}'_0$ in (11) result from the SVD of estimator $\hat{Q}' = \frac{1}{\hat{N}} S'_r \cdot S'^{\mathrm{T}}_r$. Therefore, the uncertainty associated with $\hat{U}'$ and $\hat{\bar{\Lambda}}'_0$ limit the effectiveness of the whitening transformation compared with the ideal case in which the autocorrelation matrix of $\boldsymbol{s}'_r$ is perfectly known. For the same reason, even if $\sigma'_\varepsilon$ can be chosen arbitrarily small, in practice it is pointless to choose a value lower than the largest uncertainty affecting the elements of $\hat{\bar{\Lambda}}'_0$. In any case, if $\sigma'^2_\varepsilon < \sigma^2_\varepsilon$, then the signal noise floor after disturbance whitening is certainly lower than before applying (10).

### C. Taylor Kalman Filter (TKF) description

To derive the TKF, the Taylor's series of the phasor $p(t)$ around the reference time $t_r$ is considered. In practice, the series is truncated to the second order since using higher-order terms does not lead to significant accuracy improvements [35]. Thus,

$$P(n_r) = P(r+n) \approx p_{0,r} + p_{1,r}n + p_{2,r}n^2 \tag{12}$$

where $n = -\frac{\hat{N}-1}{2},\ldots,\frac{\hat{N}-1}{2}$ and $p_{k,r} = \frac{1}{k!}\frac{1}{f_s^k}\frac{d^k p}{dt^k}\Big|_{t_r}$ for $k = 0,1,2$ are the coefficient of the phasor Taylor's series computed at time $t_r$. Assuming to a first approximation that all disturbances are made negligible by the whitening step, then each element of vector $\hat{\boldsymbol{y}}_r$ be expressed as a function of (12) as follows, i.e.

$$\hat{y}_r(n) \approx \sqrt{2}\,\frac{(p_{0,r}+p_{1,r}n+p_{2,r}n^2)e^{j\omega_0 n} + (p^*_{0,r}+p^*_{1,r}n+p^*_{2,r}n^2)e^{-j\omega_0 n}}{2} \tag{13}$$

where "*" denotes the complex conjugate operator. Thus, if the phasor Taylor's series coefficients are included into the column vector $\boldsymbol{p}_r = \left[p_{2,r}, p_{1,r}, p_{0,r}, p^*_{0,r}, p^*_{1,r}, p^*_{2,r}\right]^{\mathrm{T}}$ and the observation intervals shift by one sample at a time, the phasor dynamic can be expressed by [35]

$$\boldsymbol{p}_{r+1} = A\,\boldsymbol{p}_r \tag{14}$$

where the system matrix is

$$A = \begin{bmatrix} 1 & 0 & 0 & 0 & 0 & 0 \\ 2 & 1 & 0 & 0 & 0 & 0 \\ 1 & 1 & 1 & 0 & 0 & 0 \\ 0 & 0 & 0 & 1 & 1 & 1 \\ 0 & 0 & 0 & 0 & 1 & 2 \\ 0 & 0 & 0 & 0 & 0 & 1 \end{bmatrix}. \tag{15}$$

Moreover, by exploiting the fundamental frequency estimated through (10), expression (13) can be rearranged into a matrix form as follows, i.e.

$$\hat{\boldsymbol{y}}_r = B(\hat{\omega}_0)\,\boldsymbol{p}_r \tag{16}$$

where $B(\hat{\omega}_0) = \begin{bmatrix} B_1(\hat{\omega}_0) & B_2(\hat{\omega}_0) \end{bmatrix}$ is a $\hat{N} \times 6$ matrix consisting of the following blocks, i.e.,

$$B_1(\hat{\omega}_0) = \frac{\sqrt{2}}{2} \begin{bmatrix} \left(\frac{-\hat{N}+1}{2}\right)^2 e^{j\left(\frac{\hat{N}-1}{2}\right)\hat{\omega}_0} & \left(\frac{-\hat{N}+1}{2}\right) e^{j\left(\frac{\hat{N}-1}{2}\right)\hat{\omega}_0} & e^{j\left(\frac{\hat{N}-1}{2}\right)\hat{\omega}_0} \\ \vdots & \vdots & \vdots \\ 0 & 0 & 1 \\ \vdots & \vdots & \vdots \\ \left(\frac{\hat{N}-1}{2}\right)^2 e^{-j\left(\frac{\hat{N}-1}{2}\right)\hat{\omega}_0} & \left(\frac{\hat{N}-1}{2}\right) e^{-j\left(\frac{\hat{N}-1}{2}\right)\hat{\omega}_0} & e^{-j\left(\frac{\hat{N}-1}{2}\right)\hat{\omega}_0} \end{bmatrix} \tag{17}$$

and

$$B_2\left(\hat{\omega}_0\right)=\frac{\sqrt{2}}{2}\begin{bmatrix} e^{-j\left(\frac{\hat{N}-1}{2}\right)\hat{\omega}_0} & \left(\frac{-\hat{N}+1}{2}\right)e^{-j\left(\frac{\hat{N}-1}{2}\right)\hat{\omega}_0} & \left(\frac{-\hat{N}+1}{2}\right)^2 e^{-j\left(\frac{\hat{N}-1}{2}\right)\hat{\omega}_0} \\ \vdots & \vdots & \vdots \\ 1 & 0 & 0 \\ \vdots & \vdots & \vdots \\ e^{j\left(\frac{\hat{N}-1}{2}\right)\hat{\omega}_0} & \left(\frac{\hat{N}-1}{2}\right)e^{j\left(\frac{\hat{N}-1}{2}\right)\hat{\omega}_0} & \left(\frac{\hat{N}-1}{2}\right)^2 e^{j\left(\frac{\hat{N}-1}{2}\right)\hat{\omega}_0} \end{bmatrix} \quad (18)$$

If the data within each adjusted interval are weighted by a window function whose coefficients are arranged into a $\hat{N}\times\hat{N}$ diagonal matrix $\Omega$ (with $\Omega=I_{\hat{N}}$ if the rectangular window is used), then the weighted vector of whitened measurement data is $\boldsymbol{z}_r=\Omega\hat{\boldsymbol{y}}_r$, and the whole dynamic system that is used to build the TKF is

$$\begin{cases}\boldsymbol{p}_{r+1}=A\,\boldsymbol{p}_r+\boldsymbol{\eta}_r\\ \boldsymbol{z}_r=H\left(\hat{\omega}_0\right)\boldsymbol{p}_r+\boldsymbol{w}_r\end{cases} \quad (19)$$

where $\boldsymbol{\eta}_r$ is the column vector including the synchrophasor model errors (e.g., due to both Taylor's series truncation and possible signal components that are not included in the signal model), $H\left(\hat{\omega}_0\right)=\Omega B\left(\hat{\omega}_0\right)$ and $\boldsymbol{w}_r$ is the vector composed by the weighted samples of noise that affect the signal after disturbance whitening. Of course, the elements of $\boldsymbol{\eta}_r$ and $\boldsymbol{w}_r$ can be reasonably assumed to be uncorrelated and white. Quite importantly, the correlation in time of the elements of $\boldsymbol{w}_r$ is negligible because, even if the observation intervals are shifted by one sample at a time, the whitening transformation (10), which is performed at every iteration of the filter, refreshes the uncertainty contributions associated with $\hat{\boldsymbol{y}}_r$ at each time step.

From the Kalman filter definition applied to (19), it follows that the equations of the *prediction step* are [41]

$$\begin{cases}\hat{\boldsymbol{p}}_{r+1}^{+}=A\,\hat{\boldsymbol{p}}_r\\ \Gamma_{r+1}^{+}=A\,\Gamma_r\,A+E\end{cases} \quad (20)$$

where superscript "+" represents the one-step-ahead predicted quantities, $\Gamma_r$ is the state estimation covariance matrix and $E$ is the covariance matrix of $\boldsymbol{\eta}_r$. This matrix is constant, since the Taylor's series model errors can be assumed to be stationary and white.

In the *update step* the equations of the TKF are

$$\begin{cases}\hat{\boldsymbol{p}}_{r+1}=\hat{\boldsymbol{p}}_{r+1}^{+}+G_{r+1}(\boldsymbol{z}_r-H\hat{\boldsymbol{p}}_{r+1}^{+})\\ \Gamma_{r+1}=(I_6-G_{r+1}H)\Gamma_{r+1}^{+}\end{cases} \quad (21)$$

where

$$G_{r+1}=\Gamma_{r+1}^{+}H^T(H\Gamma_{r+1}^{+}H^T+R)^{-1} \quad (22)$$

is the so-called Kalman gain matrix and $R$ in (22) is the covariance matrix of $\boldsymbol{w}_r$.

By using the elements of $\hat{\boldsymbol{p}}_r$, it finally results that the values of synchrophasor magnitude and phase, as well as fundamental frequency and ROCOF at reference time $t_r$ are given respectively by [26]:

$$\hat{a}\left(t_r\right)=\sqrt{2}\left|\hat{p}_{0,r}\right| \qquad \hat{\varphi}\left(t_r\right)=\angle\hat{p}_{0,r} \quad (23)$$

$$\hat{f}\left(t_r\right)=f_{\text{nom}}+\frac{f_s}{2\pi\left|\hat{p}_{0,r}\right|^2}\text{Im}\left(\hat{p}_{1,r}\,\hat{p}_{0,r}^{*}\right) \quad (24)$$

$$\widehat{ROCOF}\left(t_r\right)=\frac{f_s^2}{\pi}\left\{\frac{\text{Im}\left(\hat{p}_{2,r}\,\hat{p}_{0,r}^{*}\right)}{\left|\hat{p}_{0,r}\right|^2}-\frac{\text{Re}\left(\hat{p}_{1,r}\,\hat{p}_{0,r}^{*}\right)\text{Im}\left(\hat{p}_{1,r}\,\hat{p}_{0,r}^{*}\right)}{\left|\hat{p}_{0,r}\right|^4}\right\} \quad (25)$$

where functions Re(·) and Im(·) return the real and imaginary parts of their argument, respectively. It is worth reminding that estimators (24)-(25) are quite sensitive to noise [13]. However, since the PMU reporting rate is much lower than the sampling frequency, the streams of estimated data have to be decimated accordingly. Thus, as far as the frequency and ROCOF estimates are concerned, they can be averaged over a reporting period (e.g., over about $M$ samples if the reporting rate is equal to $f_{\text{nom}}$) to further reduce the random uncertainty contributions affecting (24)-(25).

### *D. Computational complexity*

The total computational complexity of the TW-TKF is given by the sum of the computational complexity of the three main stages of the algorithm shown in Fig. 1.

- The computational complexity of the MUSIC algorithm is $O\left(N^3\right)$ [42]. In the case at hand, it is dominated by the estimation of the autocorrelation matrix and the following SVD computation, since the estimation of the normalized fundamental frequency requires just a few iterations for the reasons explained in Section III.A.
- The disturbance whitening step requires the estimation of the autocorrelation matrix $\hat{Q}'$ over the adjusted interval, the SVD of $\hat{Q}'$, the computation of matrix $\hat{W}$ through (11) and the linear transformation (10). The computational complexity of the former three sub-steps is $O\left(\hat{N}^3\right)$, and it is mainly due to matrix multiplications. Thus, the computational burden of (10), whose complexity is $O\left(\hat{N}^2\right)$, is negligible.
- Finally, recalling that the computational complexity of a Kalman filter grows cubically both with the number of state variables in the prediction step (i.e., 6 variables in the case at hand) and with the amount of data processed in the update step [43], it follows that the computational complexity of the proposed TKF is dominated by the update step. Hence, the complexity of the last step is $O\left(\hat{N}^3\right)$.

Ultimately, putting all together and recalling that $\hat{N}\approx N$, the asymptotic computational complexity of the TW-TKF algorithm is $O\left(N^3\right)$. Nevertheless, the overall processing burden is kept within reasonable limits because the TW-TKF is conceived to be applied over one-cycle-long or two-cycle-long

observation intervals and, consequently, over data records of limited size. For example, assuming a sampling frequency $f_s$ of some kHz (i.e., large enough to avoid harmonics aliasing), the number of samples $N$ to be processed in each observation intervals is just in the order of a few hundreds.

## IV. Simulation Results

In this Section, at first the harmonics rejection capability of the TW-TKF and the W-TKF is analyzed under realistic, borderline operating conditions compliant with the Standard EN 50160:2010 for MV distribution systems [44]. Two different window functions are adopted for this study, i.e. rectangular and Hann. Then, the accuracy and the responsiveness of the basic TKF (namely without applying disturbance whitening), the W-TKF, and the TW-TKF algorithms are evaluated in greater detail considering the *P Class* testing conditions specified in the IEEE/IEC Standard [8]. In all cases, the AC waveform nominal amplitude is normalized to 1 p.u., the system frequency $f_{nom}$ is 50 Hz, the PMU sampling frequency $f_s$ is 5 kHz (so that $M$=100) with results decimated over one cycle (i.e., assuming that the reporting rate is 50 frame/s) and the SNR of the acquired signal is 66 dB (i.e., about 11 effective bits). Also, the value of $\sigma'_\varepsilon$ used to compute the whitening matrix is chosen in such a way that the SNR after the whitening step can potentially be so high as 96 dB. However, due to the uncertainty affecting $\hat{Q}'$, this value tends to degrade as the number and/or the severity of the disturbances to be removed grow.

In the TKF implementation, the state estimation covariance matrix $\Gamma_0$ is initialized to large diagonal dummy values (i.e., 10). The elements of the covariance matrix $E$ in (20) result from the variations of the truncation errors of the Taylor's series coefficients between reference times $t_r$ and $t_{r+1}$, assuming that the phasor is affected by low-frequency amplitude and phase oscillations equal to 10% of the fundamental amplitude and 0.1 rad, respectively. As a result, the diagonal elements of $E$ range from about $2\times10^{-5}$ for $p_{2,r}$ and $p^*_{2,r}$ to $4\times10^{-3}$ for $p_{0,r}$ and $p^*_{0,r}$, respectively. The elements of matrix $R$ in (22) depend on both the expected noise floor after the whitening transformation and the window functions. For this reason, while in the rectangular window case the elements of the diagonal matrix $R$ are all set equal to $\sigma'^2_\varepsilon$, when a different window is used, the diagonal elements are shaped by the squares of the window function coefficients.

As far as the first kind of tests is concerned, the TVE, |FE| and |RFE| values are computed assuming that the absolute fractional off-nominal frequency deviation $|\delta|$ changes linearly between -4% and 4%, and all harmonics from the 2nd to the 25th affect the input voltage waveform. The amplitude of each harmonic is about 70% of the corresponding limit reported in the Standard EN 50160 [44], so that the overall Total Harmonic Distortion (THD) reaches the upper bound specified in the same Standard, i.e. 8%. The maximum TVE, |FE| and |RFE| values obtained with the proposed TW-TKF algorithm (solid lines) and the W-TKF one (dashed lines) resulting from 30 repeated tests over 2500 one-cycle-long ($C$ = 1) or two-cycle-long ($C$ = 2) observation intervals are plotted in Figs. 2 and 3 as a function of the off-nominal frequency deviation when the rectangular and the Hann window function, respectively, are considered. In every test the initial phase of the fundamental is increased linearly from $-\pi$ and $\pi$, while the initial phase values of the harmonics are changed randomly in the same interval with a uniform distribution.

The large sensitivity of the W-TKF technique to the off-nominal frequency deviations is visible in all cases (especially for frequency estimation), whereas this problem completely disappears with the new TW-TKF approach thanks to both observation interval adjustment and matrix coefficient tuning in (17)-(18). In fact, in the latter case all TVE, |FE| and |RFE| values are approximately constant and almost always they are much lower than those obtained with the W-TKF when the same number of cycles is observed. In addition, while in the W-TKF case the gap between the TVE, |FE| and |RFE| values may depend on the observation intervals length, the TW-TKF accuracy over two-cycle-long intervals is just slightly better than over one-cycle-long intervals regardless of the window function considered. It is worth noticing that most of the TW-TKF results obtained with the Hann and the rectangular window are generally comparable. Therefore, for the sake of brevity and considering the higher computational burden of Hann windowing, just the rectangular window with $C$ = 1 or $C$ = 2 will be used in the following to run the Monte Carlo simulations in the *P Class* testing conditions reported in the IEEE/IEC Standard. Such conditions are listed below, i.e.

- off-nominal frequency deviation within ±2 Hz;
- off-nominal frequency deviations within ±2 Hz and one harmonic at a time (from the 2nd to 50th) with amplitude equal to 1% of the fundamental;
- sinusoidal Amplitude Modulation (AM) with a modulation index equal to 0.1 and frequency equal to 2 Hz;
- sinusoidal Phase Modulation (PM) of amplitude equal to 0.1 rad and frequency equal to 2 Hz;
- larger input wideband noise such that SNR=54 dB (this condition is not included in the IEEE/IEC Standard but it allows to analyze the estimator robustness to noise);
- linear frequency ramps at a rate of ±1 Hz/s within the interval $[f_{nom} - 2\ \text{Hz}, f_{nom} + 2\ \text{Hz}]$.
- ± 10% amplitude step changes and $\pm\pi/18$ phase step changes.

Again, the initial phase of the fundamental is increased linearly between $-\pi$ and $\pi$, while the initial phase values of both harmonics and modulating tones are chosen randomly within $[-\pi, \pi]$, with a uniform distribution. Every test is repeated 100 times. Tables I and II show the maximum TVE, |FE|, and |RFE| values obtained with the basic TKF, the W-TKF and the TW-TKF algorithms using the rectangular window over one-cycle-long and two-cycle-long observation intervals, respectively. It should be noted that all the reported values are decimated over one-cycle observation intervals, as explained at the end of Section III.C. The main remarks resulting from the analysis of the data shown in Tables I and II are summarized below.

- When just the off-nominal frequency deviation is considered, the TW-TKF is the only method that meet all the IEEE/IEC Standard limits, and particularly the |FE| and the |RFE| ones over both one-cycle-long and two-cycle-long intervals. This is mainly due to the tuning of the TKF output matrix consisting of submatrices (17)-(18), since in this case no sinusoidal disturbances affect the acquired signal. The W-TKF results shown in Tables I and II are better than those reported in [12] since in this paper the noise floor is lowered

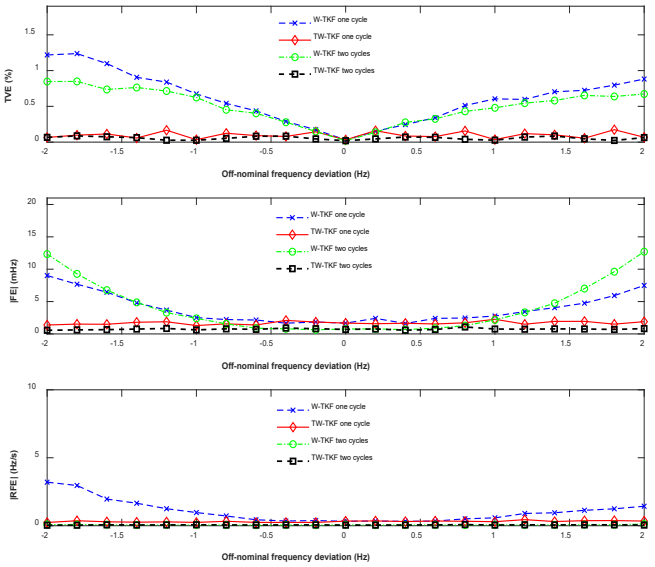


Fig. 2. Maximum TVE, |FE| and |RFE| values obtained with the W-TKF (dashed lines) and the TW-TKF (solid lines) using the rectangular window over one-cycle-long and two-cycle-long observation intervals under the joint effect of off-nominal deviations up to ±4% and 25 harmonics compliant with the EN Standard 50160:2010 with *THD*=8%.

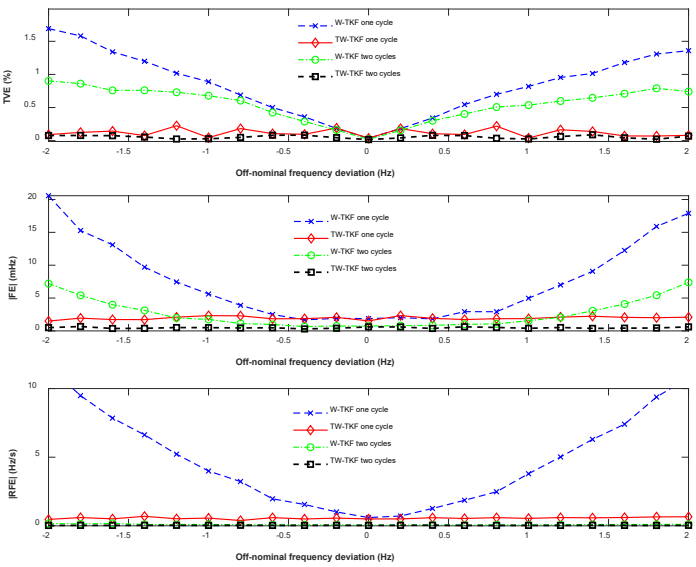


Fig. 3. Maximum TVE, |FE| and |RFE| values obtained with the W-TKF (dashed lines) and the TW-TKF (solid lines) using the Hann window over one-cycle-long and two-cycle-long observation intervals under the joint effect of off-nominal deviations up to ±4% and 25 harmonics compliant with the EN Standard 50160:2010 with *THD*=8%.

by the whitening transformation, as explained in Section III.B.

- The excellent harmonics rejection capability of the whitening-based methods shown in Fig. 2 is confirmed also by the results reported in Tables I and II. Observe that, while the TKF is sensitive to harmonics, particularly the low-order ones (as expected [12]), the W-TKF estimator greatly reduces their impact. Quite importantly, the relative impact of harmonics whitening on TKF decreases and becomes negligible as the harmonic order grows. For this reason, the results obtained with the harmonics ranging from the 4$^{th}$ to the 49$^{th}$ are omitted for the sake of brevity since they take values between those shown in the Tables for the 3$^{rd}$ and the 50$^{th}$ harmonic. The proposed TW-TKF algorithm further improves the effectiveness of disturbance whitening and synchrophasor, frequency and ROCOF estimation accuracy under the joint effect of harmonic distortion and frequency deviations. As a result, the maximum TVE, |FE| and |RFE| values are compliant with the limits specified in IEEE/IEC Standard even when one-cycle-long intervals are considered. Moreover, the results obtained when $C$=2 are just slightly lower.
- When AM or PM modulations are considered, the W-TKF and the TW-TKF algorithms still meet the IEEE/IEC standard limits in both testing conditions. However, while the maximum TVE and |RFE| values achieved with the whitening-based algorithms are generally comparable with those of the basic TKF over one-cycle-long intervals, the maximum |FE| values are considerably worse, especially in the PM case. Moreover, over two-cycle-long intervals the accuracy of both whitening-based algorithms degrades, as already reported in [34]. This behavior is due to the fact that, by prolonging the observation intervals, the whitening transformation tends to decorrelate not only the disturbances, but also the fundamental amplitude or phase modulating tones, thus decreasing the TKF capability to track amplitude and phase variations. For this reason and recalling that the computational complexity of the algorithm grows cubically with the number of samples within each interval, the proposed approach is not suitable to estimate the waveform parameters over observation intervals consisting of several cycles.
- Not surprisingly, the simulations performed without narrowband disturbances with $f_0$=$f_{nom}$ and SNR=54 dB show that the maximum TVE, |FE| and |RFE| values are visibly larger than those in the nominal case when SNR=66 dB. Indeed, even if the whitening transformation in principle replaces the noise eigenvalues with lower ones, the input wideband noise unavoidably affects the variance of estimator $\hat{Q}'$ and consequently the uncertainty associated with the estimation of its eigenvectors and eigenvalues.
- In the linear frequency ramp tests, the influence of the whitening transformation is almost negligible since no narrowband disturbances are present. However, the results obtained with the TW-TKF are globally slightly better than those achieved with the other techniques due to the joint effect of observation interval adjustment and TKF matrix elements tuning.
- Finally, the results of amplitude and phase step tests reported in Tables I and II show in most cases a significant decrease of the maximum TVE, |FE| and |RFE| values obtained with the W-TKF and TW-TKF algorithms, compared with those returned by the basic TKF. The only exceptions are the TVE values computed over two-cycle-long observation intervals. These results are unexpected because the whitening transformation is not conceived to improve estimation accuracy under transient conditions.

TABLE I

MAXIMUM TVE, |FE| AND |RFE| VALUES OBTAINED WITH THE BASIC TKF, THE W-TKF TECHNIQUE AND THE TW-TKF ALGORITHM OVER ONE-CYCLE-LONG OBSERVATION INTERVALS USING THE RECTANGULAR WINDOW IN MULTIPLE TESTING CONDITIONS. THE P CLASS LIMITS REPORTED IN THE IEEE/IEC STANDARD 60255-118-1:2018 (WHEN SPECIFIED) ARE SHOWN.

| Test Condition | $TVE_{aax}$ [%] | | | | $\|FE\|_{max}$ [mHz] | | | | $\|RFE\|_{max}$ [Hz/s] | | | |
|---|---|---|---|---|---|---|---|---|---|---|---|---|
| | *Lim.* | *C* = 1 | | | *Lim.* | *C* = 1 | | | *Lim.* | *C* = 1 | | |
| | | *TW-TKF* | *W-TKF* | *TKF* | | *TW-TKF* | *W-TKF* | *TKF* | | *TW-TKF* | *W-TKF* | *TKF* |
| Freq. Dev. only (±2 Hz) | 1 | 0.04 | 0.04 | 0.08 | 5 | 2 | 6 | 6 | 0.4 | 0.4 | 0.5 | 0.9 |
| Freq. Dev (±2Hz) + 1% 2nd Harmonic | 1 | 0.04 | 0.17 | 1.85 | 5 | 2 | 6 | 15 | 0.4 | 0.4 | 1.0 | 8.8 |
| Freq. Dev (±2Hz) + 1% 3rd Harmonic | 1 | 0.04 | 0.12 | 0.81 | 5 | 2 | 6 | 13 | 0.4 | 0.4 | 0.6 | 5.3 |
| Freq. Dev (±2Hz) + 1% 50th Harmonic | 1 | 0.04 | 0.04 | 0.19 | 5 | 2 | 6 | 6 | 0.4 | 0.4 | 0.5 | 0.7 |
| AM (2 Hz 10% modulating tone) | 3 | 0.05 | 0.06 | 0.07 | 60 | 6 | 6 | 2 | 2.3 | 0.4 | 0.4 | 0.6 |
| PM (2 Hz 0.1 rad modulating tone) | 3 | 0.05 | 0.05 | 0.07 | 60 | 26 | 26 | 3 | 2.3 | 0.6 | 0.6 | 0.6 |
| AWGN (SNR=54) | - | 0.12 | 0.12 | 0.26 | - | 7 | 7 | 9 | - | 1.0 | 1.0 | 2.6 |
| Linear freq. ramp (within ±2 Hz @±1 Hz/s) | 1 | 0.04 | 0.04 | 0.07 | 10 | 3 | 11 | 7 | 0.4 | 0.4 | 0.6 | 0.9 |
| ±10% amplitude step change | - | 6.07 | 6.05 | 8.35 | - | 220 | 210 | 710 | - | 83.0 | 86.4 | 443 |
| ±π/18 phase step change | - | 10.70 | 10.66 | 14.61 | - | 1386 | 1387 | 2750 | - | 217 | 219 | 838 |

TABLE II

MAXIMUM TVE, |FE| AND |RFE| VALUES OBTAINED WITH THE BASIC TKF, THE W-TKF TECHNIQUE AND THE TW-TKF ALGORITHM OVER TWO-CYCLE-LONG OBSERVATION INTERVALS USING THE RECTANGULAR WINDOW IN MULTIPLE TESTING CONDITIONS. THE P CLASS LIMITS REPORTED IN THE IEEE/IEC STANDARD 60255-118-1:2018 (WHEN SPECIFIED) ARE SHOWN.

| Test Condition | $TVE_{aax}$ [%] | | | | $\|FE\|_{max}$ [mHz] | | | | $\|RFE\|_{max}$ [Hz/s] | | | |
|---|---|---|---|---|---|---|---|---|---|---|---|---|
| | *Lim.* | *C* = 2 | | | *Lim.* | *C* = 2 | | | *Lim.* | *C* = 2 | | |
| | | *TW-TKF* | *W-TKF* | *TKF* | | *TW-TKF* | *W-TKF* | *TKF* | | *TW-TKF* | *W-TKF* | *TKF* |
| Freq. Dev. only (±2 Hz) | 1 | 0.02 | 0.03 | 0.04 | 5 | 0.8 | 12 | 13 | 0.4 | 0.05 | 0.07 | 0.3 |
| Freq. Dev (±2Hz) + 1% 2nd Harmonic | 1 | 0.02 | 0.10 | 0.32 | 5 | 0.8 | 13 | 15 | 0.4 | 0.06 | 0.07 | 0.4 |
| Freq. Dev (±2Hz) + 1% 3rd Harmonic | 1 | 0.02 | 0.10 | 0.17 | 5 | 0.8 | 13 | 14 | 0.4 | 0.06 | 0.07 | 0.4 |
| Freq. Dev (±2Hz) + 1% 50th Harmonic | 1 | 0.02 | 0.03 | 0.04 | 5 | 0.8 | 13 | 13 | 0.4 | 0.05 | 0.07 | 0.3 |
| AM (2 Hz 10% modulating tone) | 3 | 0.07 | 0.07 | 0.04 | 60 | 6 | 6 | 1 | 2.3 | 0.6 | 0.6 | 0.2 |
| PM (2 Hz 0.1 rad modulating tone) | 3 | 0.07 | 0.07 | 0.04 | 60 | 49 | 50 | 3 | 2.3 | 0.7 | 0.8 | 0.2 |
| AWGN (SNR=54) | - | 0.08 | 0.08 | 0.12 | - | 3 | 3 | 5 | - | 0.2 | 0.2 | 0.6 |
| Linear freq. ramp (within ±2 Hz @±1 Hz/s) | 1 | 0.03 | 0.04 | 0.03 | 10 | 2 | 25 | 12 | 0.4 | 0.1 | 0.1 | 0.3 |
| ±10% amplitude step change | - | 5.94 | 5.92 | 5.61 | - | 53 | 63 | 140 | - | 5.4 | 5.2 | 25.2 |
| ±π/18 phase step change | - | 10.42 | 10.40 | 9.86 | - | 687 | 680 | 1120 | - | 33.9 | 33.7 | 137 |

The reasons of this behavior are not fully clear. The plots showing the TVE, |FE| and |RFE| envelopes as a function of time (not reported for the space constraints) confirm not only that the maximum errors occur a few samples after the instant when the amplitude or phase step occurs, but also that the TVE, |FE| and |RFE| ripples resulting from the applications of the whitening-based techniques are usually smoother and spread over a longer time interval than those obtained with the basic TKF. For this reason, the W-TKF and TW-TKF response times associated with synchrophasor, frequency and ROCOF estimation and shown in Table III for both *C*=1 and *C*=2 cycles are approximately the same and they are roughly twice as long as those of the basic TKF. It is worth recalling that in the case of *P Class* PMUs, the response times to an input step change are defined as the time intervals elapsed between the instant when the TVE, |FE| or |RFE| values exceed a specified threshold (i.e., 1%, 5 mHz or 0.4 Hz/s, respectively) and the instant after which a new steady state is reached and such limits are no longer violated. All the response time values reported in Table III are expressed in nominal power line cycles.

TABLE III
MAXIMUM SYNCHROPHASOR, FREQUENCY AND ROCOF RESPONSE TIMES OBTAINED WITH THE BASIC TKF, THE W-TKF TECHNIQUE AND THE TW-TKF ALGORITHM OVER ONE-CYCLE-LONG AND TWO-CYCLE-LONG INTERVALS USING THE RECTANGULAR WINDOW WHEN AMPLITUDE OR PHASE STEPS OCCUR. THE P CLASS LIMITS SPECIFIED IN THE IEEE/IEC STANDARD 60255-118-1:2018 ARE ALSO SHOWN FOR THE SAKE OF COMPARISON.

| Test Condition | Window Length [cycles] | Synchrophasor response time [cycles] | | | | Frequency response time [cycles] | | | | ROCOF response time [cycles] | | | |
|---|---|---|---|---|---|---|---|---|---|---|---|---|---|
| | | Lim. | *TW-TKF* | *W-TKF* | *TKF* | Lim. | *TW-TKF* | *W-TKF* | *TKF* | Lim. | *TW-TKF* | *W-TKF* | *TKF* |
| ±10% amplitude step change | 1 | 2 | 1.55 | 1.60 | 0.96 | 4.5 | 1.90 | 1.92 | 0.98 | 6 | 1.97 | 2.00 | - |
| | 2 | 2 | 2.83 | 2.84 | 0.86 | 4.5 | 3.82 | 3.82 | 1.96 | 6 | 3.87 | 3.87 | 1.98 |
| ±π/18 phase step change | 1 | 2 | 1.81 | 1.81 | 0.98 | 4.5 | 1.95 | 1.96 | 0.98 | 6 | 2.29 | 2.31 | - |
| | 2 | 2 | 3.37 | 3.37 | 1.86 | 4.5 | 3.88 | 3.88 | 1.98 | 6 | 3.93 | 3.93 | 1.98 |

The longer transient of the whitening-based TKFs is certainly due to the fact that, even if the parameters of the fundamental component are estimated over each observation interval, two disjoint intervals are used to estimate the autocorrelation matrices needed for frequency estimation and disturbance whitening. As a result, the *P Class* response time limits specified in the IEEE/IEC Standard are fully met by the W-TKF and TW-TKF algorithm only over one-cycle-long intervals. On the other hand, even if the basic TKF exhibits a shorter latency in all step tests, its ROCOF response times over one-cycle-long intervals are undefined because the maximum |RFE| values are never steadily below the specified *P Class* limit, i.e. 0.4 Hz/s.

## V. EXPERIMENTAL RESULTS IN REAL TRANSIENT CONDITIONS

The performance of the TW-TKF, the W-TKF and the basic TKF algorithm were finally analyzed and compared using some IEEE Project Group 1159.2 experimental data records. Such data records consist of several 60-Hz three-phase waveforms acquired with a sampling rate $f_s$ = 15.360 kHz, so that $M$=256 samples per nominal cycle are collected. The signals are affected by a variety of anomalous transient events. Figs. 4(a) and 5(a) show two of such waveforms, which exhibit short voltage dips and a sudden THD increment, respectively. Figs. 4(b) and 5(b) display instead the corresponding sample-by-sample estimates of amplitude, frequency, phase, frequency and ROCOF returned by the original TKF (dotted lines), the W-TKF (dashed lines) and the TW-TKF algorithm (thick solid lines) over one-cycle-long observation intervals. The results obtained over two-cycle-long intervals are not reported because the data records and the transient events have a very short duration. Therefore, to visualize more clearly the tracking capability of the algorithms under test, the results obtained with $C$ = 1 are preferable even if the estimation accuracy is certainly worse than over two-cycle-long intervals. Quite importantly, the TVE, |FE| and |RFE| patterns are not reported in this case because the actual reference values of amplitude, phase, frequency and ROCOF are unknown and cannot be estimated with controlled uncertainty. Hence, the results shown in Figs. 4(b) and 5(b) provide just a qualitative, but significant comparison between the three algorithms under test. In this regard, it is evident that the TW-TKF algorithm ensures a very good responsiveness as well as a better accuracy and a much higher disturbance rejection capability than that of both the basic TKF and the W-TKF estimator. The performance gap is boosted by the fact that no output decimation and averaging is applied to the output streams of estimates. In fact, due to the very high sampling frequency of the original data records, the effect of noise on sample-by-sample estimates (particularly those of frequency and ROCOF) is particularly high, in accordance with the theoretical analysis reported in [13]. The fluctuations of all the estimates returned by the TW-TKF are indeed several order of magnitude smaller than those of the original TKF. Also, the TW-TKF algorithm is clearly less sensitive than the W-TKF estimator to both possible overshoots during amplitude changes (see results in Fig. 4(b)) and harmonic distortion (see amplitude estimation in Fig. 5(b)).

## VI. CONCLUSIONS

In this paper, a Tuned Whitening-based Taylor-Kalman Filter (TW-TKF) for synchrophasor magnitude, phase, frequency and ROCOF estimation is presented. The proposed algorithm improves the performance of a basic TKF in two ways, i.e.

- through a preliminary estimation of the fundamental frequency, which allows both to process the samples of an almost integer number of actual power line cycles and to tune the coefficients of the output matrix used in the update step of the TKF;
- through a linear whitening transformation conceived to decorrelate possible narrowband disturbances.

The results obtained in the *P Class* testing conditions specified in the IEEE/IEC Standard 60255-118-1-2018 show an impressive accuracy improvement in steady-state conditions, namely under the joint effect of off-nominal frequency deviation and noise even over one-cycle-long intervals. Quite unexpectedly, tangible benefits were observed even when amplitude or phase steps occur. In such conditions the peak TVE, |FE| and |RFE| values obtained with the TW-TKF approach are lower than those returned by a basic TKF, but the response times are roughly double. Nevertheless, the TW-TKF ensures full compliance with both the accuracy and response time limits specified in the IEEE/IEC Standard for *P Class* PMUs over one-cycle-long observations at a reasonable computational cost. The benefits of the TW-TKF algorithm compared with the other estimators under transient conditions are also well visible when experimental data records are used.

## APPENDIX A
## DISTURBANCE WHITENING TRANSFORMATION PROOF

Given the autocorrelation matrix $Q'$ of an input data vector

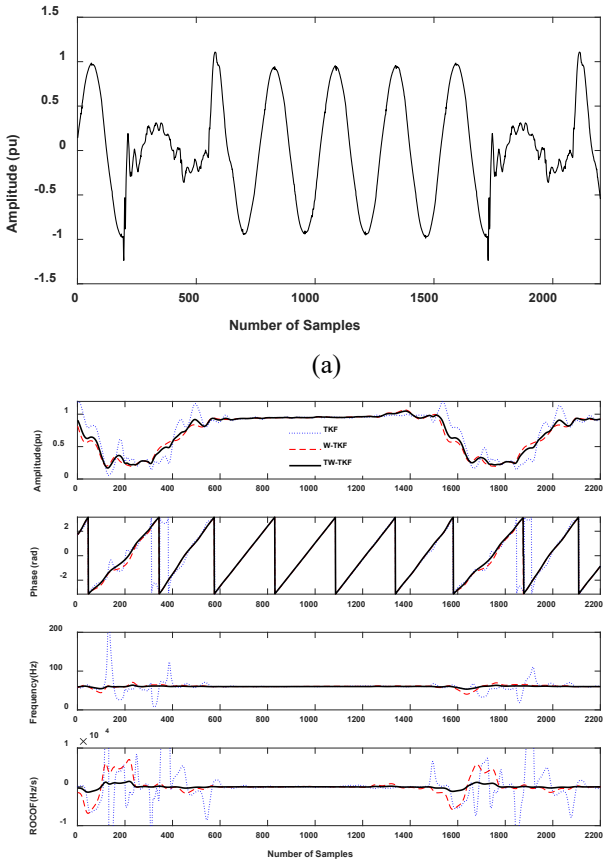


Fig. 4. Example of real voltage dips (a) and corresponding sample-by-sample amplitude, phase, frequency and ROCOF estimates (b) returned by the original TKF (dotted lines), the W-TKF (dashed lines) and the proposed TW-TKF (thick solid lines) using the rectangular window over one-cycle-long observation intervals.

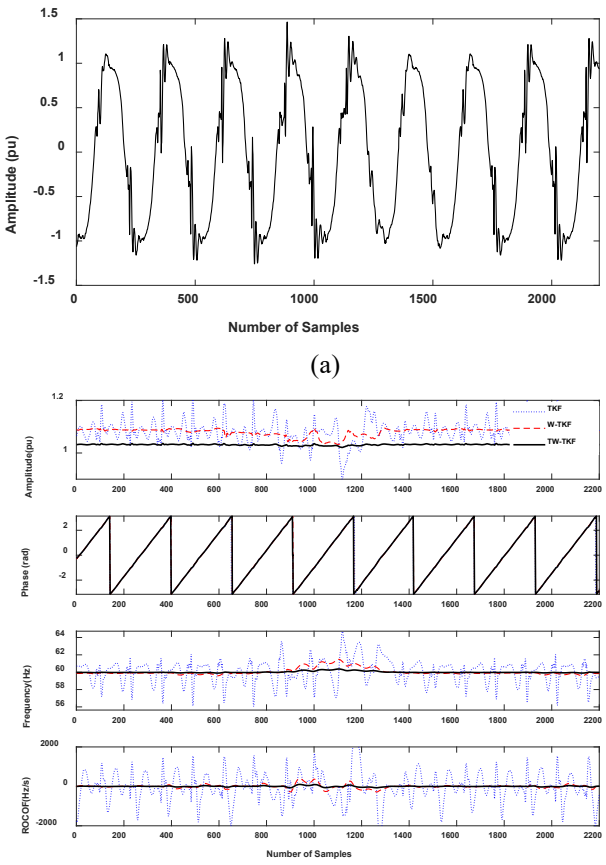


Fig. 5. Example of real sudden harmonic distortion (a) and corresponding sample-by-sample amplitude, phase, frequency and ROCOF estimates (b) returned by the original TKF (dotted lines), the W-TKF (dashed lines) and the proposed TW-TKF (thick solid lines) using the rectangular window over one-cycle-long observation intervals.

$\boldsymbol{s}'_r$ decomposed into signal and noise subspaces as expressed in (8), the purpose of disturbance whitening is to find the matrix $W$ such that the autocorrelation matrix of vector $\boldsymbol{y}_r = W \cdot \boldsymbol{s}'_r$ has the same eigenvectors of $Q'$, but it contains only the eigenvalues of the fundamental component and those of a white noise floor with power, i.e.

$$Q'_W = E\left\{\boldsymbol{y}_r \boldsymbol{y}_r^T\right\} = U' \begin{bmatrix} \Lambda_0 & 0 \\ 0 & \sigma'^2_\varepsilon I_{\hat{N}-2} \end{bmatrix} U'^{\mathrm{T}} \qquad \text{(A.1)}$$

Since $Q'_W = WQ'W^{\mathrm{T}}$ and recalling that $Q'$ is a positive semidefinite (and therefore symmetric) matrix, (A.1) can be rewritten as

$$WU' \begin{bmatrix} \Lambda_0^{\frac{1}{2}} & 0 \\ 0 & \overline{\Lambda}_0'^{\frac{1}{2}} \end{bmatrix} \begin{bmatrix} \Lambda_0^{\frac{1}{2}} & 0 \\ 0 & \overline{\Lambda}_0'^{\frac{1}{2}} \end{bmatrix} U'^{\mathrm{T}} \; W^T = U' \begin{bmatrix} \Lambda_0^{\frac{1}{2}} & 0 \\ 0 & \sigma'_\varepsilon I_{\hat{N}-2} \end{bmatrix} \begin{bmatrix} \Lambda_0^{\frac{1}{2}} & 0 \\ 0 & \sigma'_\varepsilon I_{\hat{N}-2} \end{bmatrix} U'^{\mathrm{T}} \qquad \text{(A.2)}$$

Therefore, considering just the right half of both sides of equation (A.2) and recalling that $U'^{-1} = U'^{\mathrm{T}}$ because it is orthogonal, it finally results that

$$W = U' \begin{bmatrix} I_2 & 0 \\ 0 & \sigma'_\varepsilon \overline{\Lambda}_0'^{-\frac{1}{2}} \end{bmatrix} U'^{\mathrm{T}}. \qquad \text{(A.3)}$$

## VII. References


[1] M. M. Albu, M. Sănduleac, and C. Stănescu, "Syncretic Use of Smart Meters for Power Quality Monitoring in Emerging Networks," *IEEE Trans. Smart Grid*, vol. 8, no. 1, pp. 485–492, Jan. 2017, doi: 10.1109/TSG.2016.2598547.

[2] A. Angioni, J. Shang, F. Ponci, and A. Monti, "Real-Time Monitoring of Distribution System Based on State Estimation," *IEEE Trans. Instrum. Meas.*, vol. 65, no. 10, pp. 2234–2243, Oct. 2016, doi: 10.1109/TIM.2016.2583239.

[3] A. Bashian, M. Assili, and A. Anvari-Moghaddam, "A security-based observability method for optimal PMU-sensor placement in WAMS," *Int. J. Electr. Power Energy Syst.*, vol. 121, p. 106157, Oct. 2020, doi: 10.1016/j.ijepes.2020.106157.

[4] A. Bashian, M. Assili, A. Anvari-Moghaddam, and O. R. Marouzi, "Co-optimal PMU and communication system placement using hybrid wireless sensors," *Sustain. Energy, Grids Networks*, vol. 19, Sep. 2019, doi: 10.1016/j.segan.2019.100238.

[5] R. Andreoni, D. Macii, M. Brunelli, and D. Petri, "Tri-Objective Optimal PMU Placement including Accurate State Estimation: The Case of Distribution Systems," *IEEE Access*, vol. 9, pp. 62102–62117, 2021, doi: 10.1109/ACCESS.2021.3074579.

[6] Y. Seferi, R. G. Q. Cetina, and S. M. Blair, "Review of PMU Algorithms Suitable for Real-Time Operation With Digital Sampled Value Data,"

AMPS 2021, *11th IEEE Int. Work. Appl. Meas. Power Syst.*, pp. 1–6, Sep. 2021, doi: 10.1109/AMPS50177.2021.9586034.

[7] C. Muscas and P. A. Pegoraro, "Algorithms for Synchrophasors, Frequency, and ROCOF," *Chapter 3*, Elsevier Inc., 2016, pp. 21–51.

[8] "IEEE/IEC 60255-118-1-2018 - IEEE/IEC International Standard - Measuring relays and protection equipment - Part 118-1: Synchrophasor for power system measurement, 2018." .

[9] A. Borghetti, C. A. Nucci, M. Paolone, G. Ciappi, and A. Solari, "Synchronized phasors monitoring during the islanding maneuver of an active distribution network," *IEEE Trans. Smart Grid*, vol. 2, no. 1, pp. 82–91, 2011, doi: 10.1109/TSG.2010.2094213.

[10] D. Carta, C. Muscas, P. A. Pegoraro, A. V. Solinas, and S. Sulis, "Compressive Sensing-Based Harmonic Sources Identification in Smart Grids," *IEEE Trans. Instrum. Meas.*, vol. 70, 2021, doi: 10.1109/TIM.2020.3036753.

[11] G. Barchi, D. Fontanelli, D. Macii, and D. Petri, "On the accuracy of phasor angle measurements in power networks," *IEEE Trans. Instrum. Meas.*, vol. 64, no. 5, pp. 1129–1139, May 2015, doi: 10.1109/TIM.2014.2363752.

[12] A. Bashian, D. Macii, D. Fontanelli, and D. Petri, "Kalman Filtering with Harmonics Whitening for P Class Phasor Measurement Units," AMPS 2021, *11th IEEE Int. Work. Appl. Meas. Power Syst.*, pp. 1–6, Sep. 2021, doi: 10.1109/AMPS50177.2021.9586033.

[13] D. Macii, D. Fontanelli, G. Barchi, and D. Petri, "Impact of Acquisition Wideband Noise on Synchrophasor Measurements: A Design Perspective," *IEEE Trans. Instrum. Meas.*, vol. 65, no. 10, pp. 2244–2253, Oct. 2016, doi: 10.1109/TIM.2016.2594023.

[14] D. Macii and D. Petri, "Digital filters for phasor measurement units: Design criteria, advantages and limitations," *AMPS 2019 - 10th IEEE Int. Work. Appl. Meas. Power Syst. Proc.*, Sep. 2019, doi: 10.1109/AMPS.2019.8897796.

[15] A. J. Roscoe, B. Dickerson, and K. E. Martin, "Filter Design Masks for C37.118.1a-Compliant Frequency-Tracking and Fixed-Filter M-Class Phasor Measurement Units," *IEEE Trans. Instrum. Meas.*, vol. 64, no. 8, pp. 2096–2107, Aug. 2015, doi: 10.1109/TIM.2015.2445111.

[16] A. J. Roscoe, I. F. Abdulhadi, and G. M. Burt, "P and M class phasor measurement unit algorithms using adaptive cascaded filters," *IEEE Trans. Power Deliv.*, vol. 28, no. 3, pp. 1447–1459, 2013, doi: 10.1109/TPWRD.2013.2238256.

[17] P. Romano and M. Paolone, "Enhanced interpolated-DFT for synchrophasor estimation in FPGAs: Theory, implementation, and validation of a PMU prototype," *IEEE Trans. Instrum. Meas.*, vol. 63, no. 12, pp. 2824–2836, Dec. 2014, doi: 10.1109/TIM.2014.2321463.

[18] B. Jafarpisheh, S. M. Madani, and S. Jafarpisheh, "Improved DFT-Based phasor estimation algorithm using down-sampling," *IEEE Trans. Power Deliv.*, vol. 33, no. 6, pp. 3242–3245, Dec. 2018, doi: 10.1109/TPWRD.2018.2831005.

[19] D. Belega and D. Petri, "Fast procedures for accurate parameter estimation of sine-waves affected by noise and harmonic distortion," *Digit. Signal Process.*, vol. 114, p. 103035, Jul. 2021, doi: 10.1016/J.DSP.2021.103035.

[20] J. K. Hwang, C. K. Song, and M. G. Jeong, "DFT-Based phasor estimation for removal of the effect of multiple DC components," *IEEE Trans. Power Deliv.*, vol. 33, no. 6, pp. 2901–2909, Dec. 2018, doi: 10.1109/TPWRD.2018.2825257.

[21] D. Belega and D. Petri, "Accuracy analysis of the multicycle synchrophasor estimator provided by the interpolated DFT algorithm," *IEEE Trans. Instrum. Meas.*, vol. 62, no. 5, pp. 942–953, 2013, doi: 10.1109/TIM.2012.2236777.

[22] K. Duda and T. P. Zielinski, "P Class and M Class Compliant PMU Based on Discrete-Time Frequency-Gain Transducer," *IEEE Trans. Power Deliv.*, pp. 1–1, 2021, doi: 10.1109/TPWRD.2021.3076831.

[23] A. Derviskadic, P. Romano, and M. Paolone, "Iterative-Interpolated DFT for Synchrophasor Estimation: A Single Algorithm for P-and M-Class Compliant PMUs," *IEEE Trans. Instrum. Meas.*, vol. 67, no. 3, pp. 547–558, Mar. 2018, doi: 10.1109/TIM.2017.2779378.

[24] J. A. de la O Serna, "Dynamic phasor estimates for power system oscillations," *IEEE Trans. Instrum. Meas.*, vol. 56, no. 5, pp. 1648–1657, Oct. 2007, doi: 10.1109/TIM.2007.904546.

[25] M. A. Platas-Garza and J. A. De La O Serna, "Dynamic phasor and frequency estimates through maximally flat differentiators," *IEEE Trans. Instrum. Meas.*, vol. 59, no. 7, pp. 1803–1811, Jul. 2010, doi: 10.1109/TIM.2009.2030921.

[26] D. Belega, D. Fontanelli, and D. Petri, "Dynamic phasor and frequency measurements by an improved taylor weighted least squares algorithm," *IEEE Trans. Instrum. Meas.*, vol. 64, no. 8, pp. 2165–2178, Aug. 2015, doi: 10.1109/TIM.2014.2385171.

[27] P. Tosato, D. Macii, M. Luiso, D. Brunelli, D. Gallo, and C. Landi, "A Tuned Lightweight Estimation Algorithm for Low-Cost Phasor Measurement Units," *IEEE Trans. Instrum. Meas.*, vol. 67, no. 5, pp. 1047–1057, May 2018, doi: 10.1109/TIM.2017.2775458.

[28] M. A. Platas-Garza and J. A. De La O Serna, "Dynamic harmonic analysis through Taylor-Fourier transform," *IEEE Trans. Instrum. Meas.*, vol. 60, no. 3, pp. 804–813, Mar. 2011, doi: 10.1109/TIM.2010.2064690.

[29] M. Bertocco, G. Frigo, C. Narduzzi, C. Muscas, and P. A. Pegoraro, "Compressive Sensing of a Taylor-Fourier Multifrequency Model for Synchrophasor Estimation," *IEEE Trans. Instrum. Meas.*, vol. 64, no. 12, pp. 3274–3283, Dec. 2015, doi: 10.1109/TIM.2015.2450295.

[30] R. Roy and T. Kailath, "ESPRIT—Estimation of Signal Parameters Via Rotational Invariance Techniques," *IEEE Trans. Acoust.*, vol. 37, no. 7, pp. 984–995, 1989, doi: 10.1109/29.32276.

[31] P. Stoica and A. Eriksson, "MUSIC estimation of real-valued sine-wave frequencies," *Signal Processing*, vol. 42, no. 2, pp. 139–146, Mar. 1995, doi: 10.1016/0165-1684(94)00123-H.

[32] P. Banerjee and S. C. Srivastava, "A subspace-based dynamic phasor estimator for synchrophasor application," *IEEE Trans. Instrum. Meas.*, vol. 61, no. 9, pp. 2436–2445, 2012, doi: 10.1109/TIM.2012.2190336.

[33] Z. D. Drummond, K. E. Claytor, D. R. Allee, and D. M. Hull, "An Optimized Subspace-Based Approach to Synchrophasor Estimation," *IEEE Trans. Instrum. Meas.*, vol. 70, 2021, doi: 10.1109/TIM.2020.3017059.

[34] D. Macii, G. Barchi, and D. Fontanelli, "Decorrelation-based Harmonic Distortion Reduction for Synchrophasor Measurements," *AMPS 2017 - IEEE International Workshop on Applied Measurements for Power Systems, Proceedings*, Sep. 2017, doi: 10.1109/AMPS.2017.8078321.

[35] D. Fontanelli, D. Macii, and D. Petri, "Dynamic synchrophasor estimation using Smoothed Kalman filtering," *IEEE Instrumentation and Measurement Technology Conference, May. 2016,* doi: 10.1109/I2MTC.2016.7520462.

[36] J. A. De La O Serna and J. Rodríguez-Maldonado, "Instantaneous oscillating phasor estimates with TaylorK-Kalman filters," *IEEE Trans. Power Syst.*, vol. 26, no. 4, pp. 2336–2344, Nov. 2011, doi: 10.1109/TPWRS.2011.2157539.

[37] C. Muscas, P. A. Pegoraro, S. Sulis, M. Pau, F. Ponci, and A. Monti, "New Kalman Filter Approach Exploiting Frequency Knowledge for Accurate PMU-Based Power System State Estimation," *IEEE Trans. Instrum. Meas.*, vol. 69, no. 9, pp. 6713–6722, Sep. 2020, doi: 10.1109/TIM.2020.2977744.

[38] R. Ferrero, P. A. Pegoraro, and S. Toscani, "Dynamic Synchrophasor Estimation by Extended Kalman Filter," *IEEE Trans. Instrum. Meas.*, vol. 69, no. 7, pp. 4818–4826, Jul. 2020, doi: 10.1109/TIM.2019.2955797.

[39] R. Ferrero, P. A. Pegoraro, and S. Toscani, "Synchrophasor Estimation for Three-Phase Systems Based on Taylor Extended Kalman Filtering," *IEEE Trans. Instrum. Meas.*, vol. 69, no. 9, pp. 6723–6730, Sep. 2020, doi: 10.1109/TIM.2020.2983622.

[40] Steven M. Kay, *Modern spectral estimation : theory and application*. Englewood Cliffs, N.J. : Prentice Hall, 1988.

[41] T. K. Y. Bar-Shalom, X. Rong Li, *Estimation with Applications to Tracking and Navigation: Theory Algorithms and Software | Wiley*. Hoboken, NJ, USA: Wiley, 2001.

[42] H. Zhang, H. C. Wu, and S. Y. Chang, "Novel fast MUSIC algorithm for spectral estimation with high subspace dimension," *Int. Conf. Comput. Netw. Commun. ICNC 2013*, pp. 474–478, Jan. 2013, doi: 10.1109/ICCNC.2013.6504131.

[43] D. Willner, C.-B. Chang, and K.-P. Dunn, "Kalman Filter Configurations for Multiple Radar Systems," Apr. 1976, Available online: https://apps.dtic.mil/sti/citations/ADA026367.

[44] EN Standard 50160:2010, *Voltage characteristics of electricity supplied by public electricity networks*, Belgium, Dec 2010.

**Amir Bashian** received the B.Sc. degree and M.Sc. degree from Ferdowsi University of Mashhad, Mashhad, Iran, in 2008 and 2011, respectively and the Ph.D. degree from Shahrood University of Technology, Shahrood, Iran in 2020, all in Electrical Engineering-Power Systems. He was a Visiting Researcher at the Aalborg University, Aalborg, Denmark, in 2019 and a Postdoctoral Research Fellow at the Department of Industrial Engineering, University of Trento, Trento, Italy in 2021. He is about to join the Scania R&D team, Stockholm, Sweden, as a Development Engineer. His research interests include smart grids, signal processing in power systems, wide area monitoring systems, measurement and estimation techniques, and flexible design strategies.

**David Macii** (M' 06, SM' 2014) received the M.S. degree in Electronics Engineering and the Ph.D. degree in Information Engineering from the University of Perugia, Perugia, Italy, in 2000 and in 2003, respectively. He was a visiting researcher at the University of Westminster, London, UK in 2002, at the Advanced Learning and Research Institute of the University of Lugano, Lugano, Switzerland, between 2004 and 2005 and he was a Fulbright Research Scholar at the Berkeley Wireless Research Center, University of California at Berkeley, Berkeley, USA, between 2009 and 2010.Berkeley, CA, USA. Currently, he is an Associate Professor with the Department of Industrial Engineering of the University of Trento, Trento, Italy. He is author and co-author of more than 150 papers published in books, scientific journals, and international conference proceedings. Since 2018 he has been an Editor for the journal "Measurement". His research interests are focused on measurement and estimation techniques based on digital signal processing for mechatronics applications, industrial electronics and power systems.

**Daniele Fontanelli** (M'10, SM'19) received the M.S. degree in Information Engineering in 2001, and the Ph.D. degree in Automation, Robotics and Bioengineering in 2006, both from the University of Pisa, Pisa, Italy. He was a Visiting Scientist with the Vision Lab of the University of California at Los Angeles, Los Angeles, US, from 2006 to 2007. From 2007 to 2008, he has been an Associate Researcher with the Interdepartmental Research Center ``E. Piaggio", University of Pisa. From 2008 to 2013 he joined as an Associate Researcher the Department of Information Engineering and Computer Science and from 2014 the Department of Industrial Engineering, both at the University of Trento, Trento, Italy, where he is now an Associate Professor and he is leading the EIT-Digital International Master on Autonomous Systems. He has authored and co-authored more than 150 scientific papers in peer-reviewed top journals and conference proceedings. He is currently an Associate Editor in Chief for the IEEE Transactions on Instrumentation and Measurement and an Associate Editor for the IET Science, Measurement & Technology Journal and the IEEE Robotics and Automation Letters. He has also served in the technical program committee of numerous conferences in the area of measurements and robotics. His research interests include distributed and real-time estimation and control, localization algorithms, synchrophasor estimation, clock synchronization algorithms, resource aware control, wheeled mobile robots, service robotics and human-robot interaction and estimation.

**Dario Petri** (M'92–SM'05–F'09) is a Full Professor of Measurement Science and Electronic Instrumentation and the chair of the Quality Assurance Committee of the University of Trento, Trento, Italy. He is an IEEE Fellow member and the recipient of the 2020 IEEE Joseph F. Keithley Award "for contributions to measurement fundamentals and signal processing techniques in instrumentation and measurement." He is the chair of the IEEE Smart Cities Initiative in Trento since 2015 and an Associate Editor in Chief of the IEEE Transactions on Instrumentation and Measurement. Dario Petri received the M.Sc. degree (summa cum laude) and the Ph.D. degree in electronics engineering from the University of Padua, Padua, Italy, in 1986 and 1990, respectively. He has been an author of about 350 papers published in international journals or in proceedings of peer reviewed international conferences. His research activities are focused on digital signal processing, embedded systems, measurement for quality management and fundamentals of measurement theory.